Rakenteiden Mekaniikka (Journal of Structural Mechanics)
Vol. 44, No 3, 2011, pp. 156 – 171

Thermodynamic interpretation of finite volume algorithms

Arkadi Berezovski

Summary. The thermodynamic consistency is a desired feature of numerical algorithms for physical problems. Such a consistency can be achieved if the computational cells are considered as discrete thermodynamic systems. It is shown that faithful, accurate, and conservative finite-volume algorithms are compatible with thermodynamics through the identification of numerical fluxes and excess quantities. One-dimensional wave propagation and heat conduction are considered as examples.

Key words: conservation laws, finite-volume methods, thermodynamics

Introduction

Finite volume methods are broadly applied to the solution of systems of hyperbolic conservation laws (Godlewski and Raviart, 1996; Toro, 1997, 2001; LeVeque, 2002; Guinot, 2003) due to their physical soundness and accuracy. The main idea of such methods is the control of conservation laws on each finite volume cell in the computational domain. However, the division of a body into a finite number of computational cells requires the description of all fields inside the cells as well as on the interaction between neighboring cells. It is desired that the corresponding description should be thermodynamically consistent.

Thermodynamic notions can be introduced if a cell is considered as a thermodynamic system. This means that the thermodynamic state of the cell should be clearly defined. In the local equilibrium approximation, all notions of classical thermodynamics are valid for quantities averaged over the cell. However, averaging of wanted fields inside the cell leads to discontinuities of the fields at boundaries between cells. This also leads to the appearance of excess quantities, which represent the difference between exact and approximate values of the fields. The interaction between neighboring cells can be described by means of fluxes at the boundaries of the cells. Therefore, the correspondence between fluxes and excess quantities is needed to be established.

In what follows, we consider a method of attack the problem on the example of the construction of numerical schemes for conservation laws. Linear elastic wave propagation and heat conduction are chosen as representative cases due to their simplicity and broad applicability. The one-dimensional setting is used for convenience.

The paper is organized as follows. Examples of conservation laws are presented in the next section. General solution for the linear elastic case has been described then since it is used in the construction of the finite volume wave-propagation algorithm. The algorithm itself is presented on the example of linear elasticity. The alternative thermodynamic interpretation of the construction of the algorithm is described in the following section.

In the last section, it is shown that similar thermodynamic construction leads to the well-known algorithm also in the case of heat conduction.

Examples of conservation laws

Conservation laws are time-dependent systems of partial differential equations (usually nonlinear) with a particularly simple structure. In one space dimension the equations take the form

$$\frac{\partial}{\partial t}\mathbf{q}(x,t) + \frac{\partial}{\partial x} f(\mathbf{q}(x,t)) = 0, \tag{1}$$

where t is time, x is space variable, $\mathbf{q}$ is a vector of conserved quantities, and $f(\mathbf{q})$ is called the flux function. If the problem is assumed to be hyperbolic, hence the Jacobian $f'(\mathbf{q})$ has real eigenvalues and a complete set of eigenvectors.

The following examples represent the formulation of various problems in terms of conservation laws.

Euler equations of gas dynamics

It is well known (Thompson, 1972, e.g.) that gas dynamic flows are governed by the following conservation laws:
Balance of mass:

$$\frac{\partial \rho}{\partial t} + \frac{\partial \rho v}{\partial x} = 0. \tag{2}$$

Balance of linear momentum (no body forces):

$$\frac{\partial \rho v}{\partial t} + \frac{\partial (\rho v^2 + p)}{\partial x} = 0. \tag{3}$$

Balance of energy:

$$\frac{\partial \rho e}{\partial t} + \frac{\partial v(\rho e + p)}{\partial x} = 0. \tag{4}$$

Here $\rho = \rho(x,t)$ is the density, v is the velocity, ρv is the momentum, e is the specific internal energy, and p is pressure. The pressure p is given by a known function of the other state variables (the specific functional relation depends on the gas and is called the "equation of state").

Shallow water equations

The governing equations for shallow water are slightly simpler (Stoker, 1957):
Balance of mass:

$$\frac{\partial h}{\partial t} + \frac{\partial h v}{\partial x} = 0. \tag{5}$$

Balance of linear momentum:

$$\frac{\partial h v}{\partial t} + \frac{\partial (h v^2 + \frac{1}{2} g h^2)}{\partial x} = 0. \tag{6}$$

Here $h(x,t)$ is the fluid depth, g is the gravitational acceleration. This nonlinear system of conservation laws is similar to the Euler equations of gas dynamics but with depth playing the role of density.

Heat conduction equation

The heat conduction equation is based on the balance of energy (Lienhard and Lienhard, 2004):

$$\frac{\partial \rho e}{\partial t} + \frac{\partial q}{\partial x} = 0, \tag{7}$$

where q is the heat flux.

In the simplest case, the specific internal energy is proportional to temperature

$$e = C_p \theta, \tag{8}$$

where θ is temperature and C_p is the heat capacity of the material.

Applying the Fourier's law of heat conduction

$$q = -k \frac{\partial \theta}{\partial x}, \tag{9}$$

where $k(x)$ is the coefficient of thermal conductivity, we arrive at the one-dimensional heat conduction equation

$$\rho C_p \frac{\partial \theta}{\partial t} - \frac{\partial}{\partial x}\left(k \frac{\partial \theta}{\partial x}\right) = 0. \tag{10}$$

Linear elasticity

In the linear elasticity (Achenbach, 1973), the balance of linear momentum

$$\rho(x) \frac{\partial v}{\partial t} - \frac{\partial \sigma}{\partial x} = 0, \tag{11}$$

is complemented by the kinematic compatibility condition

$$\frac{\partial \varepsilon}{\partial t} - \frac{\partial v}{\partial x} = 0, \tag{12}$$

and the stress-strain relation in the form of the Hooke's law

$$\sigma = (\lambda + 2\mu)\varepsilon, \tag{13}$$

where $\rho(x)$ is the matter density, $v(x,t)$ is the particle velocity, $\sigma(x,t)$ is the uniaxial stress, λ and μ are Lamé coefficients, and $\varepsilon(x,t)$ is a measure of the uniaxial strain.

General solution in the linear elastic case

The conservation law (1) in the case of linear elasticity can be expressed in the form

$$\frac{\partial}{\partial t}\mathbf{q}(x,t) + \mathbf{A}\frac{\partial}{\partial x}\mathbf{q}(x,t) = 0, \tag{14}$$

where the matrix $\mathbf{A}$ corresponds to the system of Eqs. (11) – (13)

$$\mathbf{A} = \begin{pmatrix} 0 & -1/\rho \\ -\rho c^2 & 0 \end{pmatrix}, \quad \text{and} \quad \mathbf{q}(x,t) = \begin{pmatrix} \varepsilon \\ \rho v \end{pmatrix}, \tag{15}$$

and $c = \sqrt{(\lambda + 2\mu)/\rho}$ is the velocity of elastic wave.

For hyperbolic conservation laws the matrix $\mathbf{A}$ is diagonalizable, i.e.

$$\mathbf{R}^{-1}\mathbf{A}\mathbf{R} = \mathbf{\Lambda}, \tag{16}$$

where $\mathbf{R} = |r^1|r^2|$ is the eigenvector matrix and $\mathbf{\Lambda} = \mathrm{diag}(\lambda^I, \lambda^{II})$. In the case of linear elasticity, the eigenvector matrix and its inverse are

$$\mathbf{R} = \begin{pmatrix} 1 & 1 \\ Z & -Z \end{pmatrix}, \quad \mathbf{R}^{-1} = \frac{1}{2Z}\begin{pmatrix} Z & 1 \\ Z & -1 \end{pmatrix}, \tag{17}$$

where $Z = \rho c$ is impedance.

Correspondingly, the diagonalized matrix $\mathbf{\Lambda}$ is the following one

$$\mathbf{\Lambda} = \begin{pmatrix} \lambda^I & 0 \\ 0 & \lambda^{II} \end{pmatrix} = \begin{pmatrix} -c & 0 \\ 0 & c \end{pmatrix}. \tag{18}$$

It easy to see that the conservation law (14) can be represented as

$$\mathbf{R}^{-1}\frac{\partial}{\partial t}\mathbf{q}(x,t) + \mathbf{R}^{-1}\mathbf{A}\mathbf{R}\mathbf{R}^{-1}\frac{\partial}{\partial x}\mathbf{q}(x,t) = 0, \tag{19}$$

and then rewritten in the characteristic form

$$\frac{\partial}{\partial t}\mathbf{w} + \mathbf{\Lambda}\frac{\partial}{\partial x}\mathbf{w} = 0, \tag{20}$$

where $\mathbf{w} = \mathbf{R}^{-1}\mathbf{q}$ is introduced. The system of equations (20) consists of two decoupled equations for the components of the vector $\mathbf{w}$

$$\frac{\partial w^I}{\partial t} - c\frac{\partial w^I}{\partial x} = 0, \quad \frac{\partial w^{II}}{\partial t} + c\frac{\partial w^{II}}{\partial x} = 0, \tag{21}$$

solution of which are left-going and right-going waves

$$w^I(x,t) = w^I(x+ct), \quad w^{II}(x,t) = w^{II}(x-ct). \tag{22}$$

Therefore, the general solution of the system of equation (14) is their linear combination by means of eigenvectors

$$\mathbf{q}(x,t) = \mathbf{R}\mathbf{w}(x,t) = w^I(x,t)\begin{pmatrix} 1 \\ Z \end{pmatrix} + w^{II}(x,t)\begin{pmatrix} 1 \\ -Z \end{pmatrix}. \tag{23}$$

This decomposition will be used in the construction of numerical methods. To be more precise, we consider the finite-volume method for the linear elasticity.

Example of finite volume methods: wave-propagation algorithm

In the presentation of the one-dimensional wave-propagation algorithm we will follow LeVeque (2002).

Averaged quantities

Let us introduce a computational grid of cells $C_n = [x_n, x_{n+1}]$ with interfaces $x_n = n\Delta x$ and time levels $t_k = k\Delta t$. For simplicity, the grid size Δx and time step Δt are assumed to be constant. Integration Eq. (1) over the control volume $C_n \times [t_k, t_{k+1}]$ gives

$$\int_{\Delta x} \mathbf{q}(x, t_{k+1}) d\, x - \int_{\Delta x} \mathbf{q}(x, t_k) d\, x + \\ + \int_{t_k}^{t_{k+1}} \mathbf{A}\mathbf{q}(x_{n+1}, t)\, dt - \int_{t_k}^{t_{k+1}} \mathbf{A}\mathbf{q}(x_n, t)\, dt = 0. \tag{24}$$

Equation (24) can be rewritten as a numerical scheme in the flux-differencing form

$$\mathbf{Q}_n^{k+1} = \mathbf{Q}_n^k - \frac{\Delta t}{\Delta x}(\mathbf{F}_{n+1}^k - \mathbf{F}_n^k) \tag{25}$$

after introducing the average $\mathbf{Q}_n$ of the exact solution on C_n at the time $t = t_k$ and the numerical flux $\mathbf{F}_n$ that approximates the time average of the exact flux taken at the interface between the cells C_{n-1} and C_n, i.e.

$$\mathbf{Q}_n \approx \frac{1}{\Delta x} \int_{x_n}^{x_{n+1}} \mathbf{q}(x, t_k) dx, \quad \mathbf{F}_n \approx \frac{1}{\Delta t} \int_{t_k}^{t_{k+1}} \mathbf{A}\mathbf{q}(x_n, t) dt. \tag{26}$$

In general, however, the time integrals in the right-hand side of (24) cannot be evaluated exactly since $\mathbf{q}(x_n, t)$ varies with time along each edge of the cell. A fully discrete method follows from an approximation this average flux based on the values $\mathbf{Q}_n$.

Numerical fluxes

Numerical fluxes $\mathbf{F}_n$ are determined by means of the solution of the Riemann problem at interfaces between cells. The solution of the Riemann problem (at the interface between cells $n-1$ and n) consists of two waves, which we denote, following LeVeque (2002), $\mathcal{W}_n^I$ and $\mathcal{W}_n^{II}$. The left-going wave $\mathcal{W}_n^I$ moves into cell $n-1$, the right-going wave $\mathcal{W}_n^{II}$ moves into cell n (Fig. 1). The state between the two waves must be continuous across the

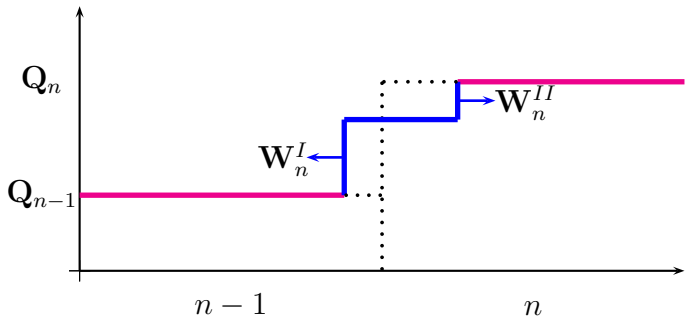

Figure 1. Left-going and the right-going waves.

interface (Rankine-Hugoniot condition) (LeVeque, 2002):

$$\mathcal{W}_n^I + \mathcal{W}_n^{II} = \mathbf{Q}_n - \mathbf{Q}_{n-1}. \tag{27}$$

In the linear case, the considered waves are determined by eigenvectors of the matrix $\mathbf{A}$ (LeVeque, 2002):

$$\mathcal{W}_n^I = \gamma_n^I \mathbf{r}_{n-1}^I, \quad \mathcal{W}_n^{II} = \gamma_n^{II} \mathbf{r}_n^{II}. \tag{28}$$

This means that Eq. (27) is represented as

$$\gamma_n^I \mathbf{r}_{n-1}^I + \gamma_n^{II} \mathbf{r}_n^{II} = \mathbf{Q}_n - \mathbf{Q}_{n-1}. \tag{29}$$

Substituting the eigenvectors into Eq. (29), we have

$$\gamma_n^I \begin{pmatrix} 1 \\ Z_{n-1} \end{pmatrix} + \gamma_n^{II} \begin{pmatrix} 1 \\ -Z_n \end{pmatrix} = \mathbf{Q}_n - \mathbf{Q}_{n-1}. \tag{30}$$

In the case of linear elasticity Eq. (30) has the form

$$\begin{pmatrix} 1 & 1 \\ \rho_{n-1} c_{n-1} & -\rho_n c_n \end{pmatrix} \begin{pmatrix} \gamma_n^I \\ \gamma_n^{II} \end{pmatrix} = \begin{pmatrix} \bar{\varepsilon}_n - \bar{\varepsilon}_{n-1} \\ \rho_n \bar{v}_n - \rho_{n-1} \bar{v}_{n-1} \end{pmatrix}. \tag{31}$$

Solving the system of linear Eqs. (31), we obtain the amplitudes of left-going and right-going waves. Then the numerical fluxes are determined as follows

$$\mathbf{F}_{n+1}^k = -\lambda_{n+1}^I \mathcal{W}_{n+1}^I = -c_{n+1} \gamma_{n+1}^I \mathbf{r}_n^I, \tag{32}$$

$$\mathbf{F}_n^k = \lambda_n^{II} \mathcal{W}_n^{II} = -c_n \gamma_n^{II} \mathbf{r}_n^{II}. \tag{33}$$

Finally, the Godunov-type numerical scheme is expressed in the form

$$\mathbf{Q}_n^{k+1} = \mathbf{Q}_n^k + \frac{\Delta t}{\Delta x} \left(c_{n+1} \gamma_{n+1}^I \mathbf{r}_n^I - c_n \gamma_n^{II} \mathbf{r}_n^{II} \right). \tag{34}$$

This is the standard form for the wave-propagation algorithm (LeVeque, 2002).

Second order corrections

The scheme considered above is formally first-order accurate only. The Godunov scheme exhibits strong numerical dissipation, and discontinuities in the solution are smeared causing low accuracy. In order to increase the order of accuracy, the correction terms are introduced as follows (LeVeque, 2002)

$$\mathcal{F}_n = \frac{1}{2} \sum_p |\lambda^p| \left(1 - \frac{\Delta t}{\Delta x} |\lambda^p| \right) W_n^p. \tag{35}$$

The obtained Lax-Wendroff scheme,

$$\mathbf{Q}_n^{k+1} - \mathbf{Q}_n^k = \frac{\Delta t}{\Delta x} (\mathbf{F}_{n+1}^k - \mathbf{F}_n^k) - \frac{\Delta t}{\Delta x} \left(\mathcal{F}_{n+1}^k - \mathcal{F}_n^k \right), \tag{36}$$

is more accurate in smooth parts of the solution, but near discontinuities, numerical dispersion generates oscillations also reducing the accuracy. A successful approach to suppress these oscillations is to apply flux limiters (LeVeque, 1997, 1998; Fogarthy and LeVeque, 1999).

Conservative wave propagation algorithm

Another possibility to increase the accuracy on smooth solutions is the conservative wave propagation algorithm (Bale et al., 2003). Here the solution of the generalized Riemann problem is obtained by means of the decomposition of the flux difference $\mathbf{A}_n\mathbf{Q}_n - \mathbf{A}_{n-1}\mathbf{Q}_{n-1}$ instead of the decomposition (27)

$$\mathcal{L}_n^I + \mathcal{L}_n^{II} = \mathbf{A}_n\mathbf{Q}_n - \mathbf{A}_{n-1}\mathbf{Q}_{n-1}. \tag{37}$$

The fluxes $\mathcal{L}^I$ and $\mathcal{L}^{II}$ are still proportional to the eigenvectors of the matrix $\mathbf{A}$

$$\mathcal{L}_n^I = \beta_n^I \mathbf{r}_{n-1}^I, \quad \mathcal{L}_n^{II} = \beta_n^{II}\mathbf{r}_n^{II}, \tag{38}$$

and the corresponding numerical scheme has the form

$$\mathbf{Q}_n^{k+1} - \mathbf{Q}_n^k = -\frac{\Delta t}{\Delta x}\left((\mathcal{L}^{II})_n^k + (\mathcal{L}^I)_{n+1}^k\right). \tag{39}$$

Coefficients β^I and β^{II} are determined from the solution of the system of linear equations (37), which reduces in the linear elastic case to

$$\begin{pmatrix} 1 & 1 \\ \rho_{n-1}c_{n-1} & -\rho_n c_n \end{pmatrix}\begin{pmatrix} \beta_n^I \\ \beta_n^{II} \end{pmatrix} = \begin{pmatrix} -(\bar{v}_n - \bar{v}_{n-1}) \\ -(\rho_n c_n^2 \bar{\varepsilon}_n - \rho_{n-1}c_{n-1}^2\bar{\varepsilon}_{n-1}) \end{pmatrix}. \tag{40}$$

As it is shown (Bale et al., 2003), the obtained algorithm is conservative and second-order accurate on smooth solutions.

The wave-propagation method was successfully applied to the simulation of wave propagation in inhomogeneous media with rapidly-varying properties with some additional modifications to ensure the full second order accuracy (LeVeque, 1997, 1998; Fogarthy and LeVeque, 1999). The advantages of the wave-propagation algorithm are high-resolution (Bale et al., 2003) and the possibility for a natural extension to higher dimensions (Langseth and LeVeque, 2000).

Local equilibrium approximation

In solid mechanics, hyperbolic conservation laws relate to the wave and front propagation, which is characterized by the values of the velocity of the order of 1000 m/s. The corresponding characteristic time is of the order of hundreds or even tens of microseconds, especially in the impact induced events. It is difficult to expect that the corresponding states of material points during such fast processes are equilibrium ones. The hypothesis of local equilibrium is commonly used to avoid the troubles with non-equilibrium states.

However, any numerical procedure supposes the division of the continuous body into a finite collection of sub-bodies, and the local equilibrium hypothesis should be extended on the whole sub-body to characterize its thermodynamic state. Moreover, all these sub-bodies interact with each other.

Often the mesh refinement is required to resolve the troubles with high gradients or simply to show that the results are independent of the mesh. If we refine the mesh, a sub-body considered as a system in local equilibrium in the sense of the coarse mesh, should be at the same time a compound system, composed by a number of local-equilibrium subsystems (sub-bodies) in the sense of the fine mesh. This dual representation of the same system results in the appearance of excess quantities in the local equilibrium description as it is shown in (Muschik and Berezovski, 2004).

Numerical methods (including finite volume methods) deal with approximated values of field variables. In finite volume methods such an approximation is achieved by simple averaging over the computational cell. This means that the value of any extensive quantity A is the sum of its averaged counterpart $\bar{A}$ and its excess part A_{ex},

$$A = \bar{A} + A_{ex}. \tag{41}$$

However, the introduced excess quantities are useless (and even superfluous) until the rules of their treatment are specified.

Excess quantities and numerical fluxes

The splitting of the body into a finite number of computational cells and averaging all the fields over the cell volumes leads to a situation, which is known in thermodynamics as "endoreversible system" (Hoffmann, Burzler and Schubert, 1997). This means that even if the state of each computational cell can be associated with a corresponding local equilibrium state (and, therefore, temperature and entropy can be defined as usual), the state of the whole body is a non-equilibrium one.

In the admitted non-equilibrium description (Muschik and Berezovski, 2004), variables are represented as the sum of averaged (local equilibrium) and excess parts:

$$\sigma = \bar{\sigma} + \Sigma \qquad v = \bar{v} + \mathcal{V}. \tag{42}$$

Here overbars still denote averaged quantity and Σ and $\mathcal{V}$ are the corresponding excess quantities.

Integrating the balance of linear momentum (11) over the computational cell gives:

$$\rho \frac{\partial}{\partial t} \int_{x_n}^{x_{n+1}} v dx = \sigma_n^+ - \sigma_n^- = \overline{\sigma}_n + \Sigma_n^+ - \overline{\sigma}_n - \Sigma_n^- = \Sigma_n^+ - \Sigma_n^-, \tag{43}$$

where superscripts "+" and "-" denote values of the quantities at right and left boundaries of the cell, respectively. Similarly, the kinematic compatibility (12) leads to

$$\frac{\partial}{\partial t} \int_{x_n}^{x_{n+1}} \varepsilon dx = v_n^+ - v_n^- = \overline{v}_n + \mathcal{V}_n^+ - \overline{v}_n - \mathcal{V}_n^- = \mathcal{V}_n^+ - \mathcal{V}_n^-. \tag{44}$$

The definition of averaged quantities

$$\overline{\rho v}_n = \frac{1}{\Delta x} \int_{x_n}^{x_{n+1}} \rho(x, t_k) v(x, t_k) dx, \quad \overline{\varepsilon}_n = \frac{1}{\Delta x} \int_{x_n}^{x_{n+1}} \varepsilon(x, t_k) dx, \tag{45}$$

allows us rewrite a first-order Godunov-type scheme (25) in terms of excess quantities

$$(\overline{\rho v})_n^{k+1} - (\overline{\rho v})_n^k = \frac{\Delta t}{\Delta x} \left(\Sigma_n^+ - \Sigma_n^- \right), \tag{46}$$

$$\bar{\varepsilon}_n^{k+1} - \bar{\varepsilon}_n^k = \frac{\Delta t}{\Delta x} \left(\mathcal{V}_n^+ - \mathcal{V}_n^- \right). \tag{47}$$

Here the superscript k denotes time step and the subscript n denotes the number of computational cell.

Though the excess quantities are determined formally everywhere inside computational cells, we need to know their values only at the boundaries of the cells, where they play the

role of numerical fluxes. To determine the values of excess quantities at the boundaries between computational cells we apply the non-equilibrium jump relations (Berezovski, Engelbrecht and Maugin, 2008). The excess stress Σ is related to the averaged stress by the non-equilibrium jump relation in bulk, which is reduced in the isothermal case to

$$[\![\bar{\sigma} + \Sigma]\!] = 0. \tag{48}$$

Here $[\![A]\!] = A^+ - A^-$, and $A^\pm$ are the uniform limits of the field A in approaching the boundary from its positive and negative sides, respectively. The same condition follows from the jump relation for the linear momentum, because the boundary between computational cells does not move.

Similarly, the jump relation following from the kinematic compatibility reads

$$[\![\bar{v} + \mathcal{V}]\!] = 0. \tag{49}$$

It is instructive to represent the non-equilibrium jump relation (48) in the numerical form

$$(\Sigma^+)_{n-1} - (\Sigma^-)_n = (\bar{\sigma})_n - (\bar{\sigma})_{n-1}, \tag{50}$$

which is illustrated in Fig. 2.

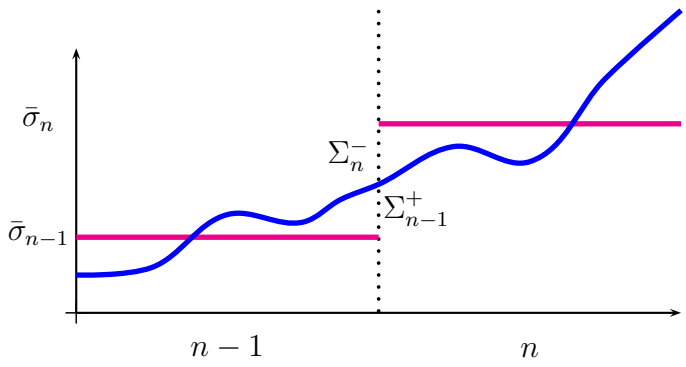

Figure 2. Stresses in the bulk.

This means that the jump condition (48) can be considered as the *continuity of the genuine unknown field* at the boundaries between computational cells. The values of excess stresses and excess velocities at the boundaries between computational cells are not independent. To demonstrate that, we consider the solution of the Riemann problem at the interface between cells.

Riemann invariants

In the one-dimensional homogeneous case, the kinematic compatibility and balance of linear momentum

$$\frac{\partial \varepsilon}{\partial t} = \frac{\partial v}{\partial x}, \tag{51}$$

$$\rho \frac{\partial v}{\partial t} = \frac{\partial \sigma}{\partial x}, \tag{52}$$

complemented by the linear constitutive relation

$$\sigma = \rho c^2 \varepsilon, \tag{53}$$

can be represented in the form

$$\frac{\partial \sigma}{\partial t} - \rho c^2 \frac{\partial v}{\partial x} = 0, \tag{54}$$

$$\rho \frac{\partial v}{\partial t} - \frac{\partial \sigma}{\partial x} = 0. \tag{55}$$

Multiplying Eq. (55) by c we can rewrite the system of Eqs. (54) – (55) as follows

$$\frac{\partial \sigma}{\partial t} - \rho c^2 \frac{\partial v}{\partial x} = 0, \tag{56}$$

$$\rho c \frac{\partial v}{\partial t} - c \frac{\partial \sigma}{\partial x} = 0. \tag{57}$$

Summing up the last two equations and subtracting the first from the second, we obtain the *characteristic form* of this system of equations

$$\frac{\partial}{\partial t}(\rho c v + \sigma) - c \frac{\partial}{\partial x}(\rho c v + \sigma) = 0, \tag{58}$$

$$\frac{\partial}{\partial t}(\rho c v - \sigma) + c \frac{\partial}{\partial x}(\rho c v - \sigma) = 0. \tag{59}$$

Denoting $Y = \rho c v + \sigma, Z = \rho c v - \sigma$, we can rewrite the system of Eqs. (58) – (59) as follows

$$\frac{\partial Y}{\partial t} - c \frac{\partial Y}{\partial x} = 0, \tag{60}$$

$$\frac{\partial Z}{\partial t} + c \frac{\partial Z}{\partial x} = 0. \tag{61}$$

The last two equations possess general solutions

$$Y = f(x + ct), \quad Z = g(x - ct) \quad \forall f, g. \tag{62}$$

The lines $x \pm ct = const$ are called as *characteristic lines*, and Y and Z are called as *Riemann invariants*, because they are conserved along characteristic lines.

Any solution of the system of Eqs. (54) – (55) can be constructed from the two Riemann invariants

$$\sigma = \frac{1}{2}(Y - Z), \tag{63}$$

$$\rho c v = \frac{1}{2}(Y + Z). \tag{64}$$

Riemann problem

The *Riemann problem* at the boundary between computational cells consists of piecewise constant initial data for the system of Eqs. (54) – (55) (Fig. 3)

$$\begin{cases} v(x) = \bar{v}_{n-1}, \quad \sigma(x) = \bar{\sigma}_{n-1}, & \text{if} \quad x < x_n; \\ v(x) = \bar{v}_n, \quad \sigma(x) = \bar{\sigma}_n, & \text{if} \quad x > x_n. \end{cases} \tag{65}$$

The solution to the Riemann problem is constructed by means of values of the Riemann invariants. At the boundary between cells

$$Y = \rho c v + \sigma = \rho_n c_n \bar{v}_n + \bar{\sigma}_n, \tag{66}$$

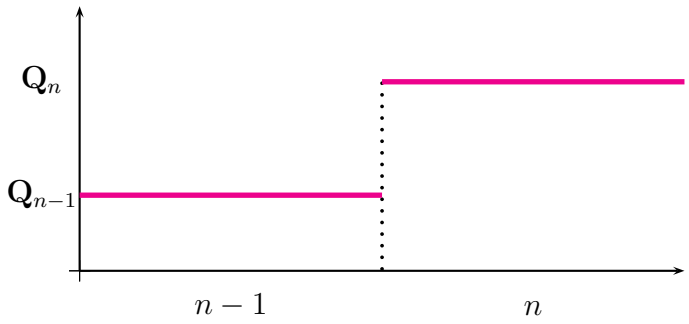

Figure 3. Riemann problem.

$$Z = \rho c v - \sigma = \rho_{n-1} c_{n-1} \bar{v}_{n-1} - \bar{\sigma}_{n-1}. \tag{67}$$

Inserting the relations (42) into the expression for the Riemann invariants at the interface (66) – (67), we obtain

$$Y = \rho c v + \sigma = \rho_n c_n \bar{v}_n + \rho_n c_n \mathcal{V}_n^- + \bar{\sigma}_n + \Sigma_n^- = \rho_n c_n \bar{v}_n + \bar{\sigma}_n, \tag{68}$$

$$Z = \rho c v - \sigma = \rho_{n-1} c_{n-1} \bar{v}_{n-1} + \rho_{n-1} c_{n-1} \mathcal{V}_n^+ - \bar{\sigma}_{n-1} - \Sigma_{n-1}^+ = \tag{69}$$

$$= \rho_{n-1} c_{n-1} \bar{v}_{n-1} - \bar{\sigma}_{n-1}.$$

It follows immediately that

$$\rho_n c_n \mathcal{V}_n^- + \Sigma_n^- \equiv 0, \tag{70}$$

$$\rho_{n-1} c_{n-1} \mathcal{V}_{n-1}^+ - \Sigma_{n-1}^+ \equiv 0, \tag{71}$$

i.e., the excess quantities depend on each other at the cell boundary.

Excess quantities at the boundaries between cells

Rewriting the jump relations (48), (49) in the form

$$(\Sigma^+)_{n-1} - (\Sigma^-)_n = (\bar{\sigma})_n - (\bar{\sigma})_{n-1}, \tag{72}$$

$$(\mathcal{V}^+)_{n-1} - (\mathcal{V}^-)_n = (\bar{v})_n - (\bar{v})_{n-1}. \tag{73}$$

and using the dependence between excess quantities (Eqs. (70) and (71)), we obtain then the system of linear equations for the determination of the excess velocities

$$\mathcal{V}_{n-1}^+ - \mathcal{V}_n^- = \bar{v}_n - \bar{v}_{n-1}, \tag{74}$$

$$\mathcal{V}_{n-1}^+ \rho_{n-1} c_{n-1} + \mathcal{V}_n^- \rho_n c_n = \rho_n c_n^2 \bar{\varepsilon}_n - \rho_{n-1} c_{n-1}^2 \bar{\varepsilon}_{n-1}. \tag{75}$$

In matrix notation the latter system of equations has the form

$$\begin{pmatrix} 1 & 1 \\ \rho_{n-1} c_{n-1} & -\rho_n c_n \end{pmatrix} \begin{pmatrix} -\mathcal{V}_{n-1}^+ \\ \mathcal{V}_n^- \end{pmatrix} = \begin{pmatrix} -(\bar{v}_n - \bar{v}_{n-1}) \\ -(\rho_n c_n^2 \bar{\varepsilon}_n - \rho_{n-1} c_{n-1}^2 \bar{\varepsilon}_{n-1}) \end{pmatrix}. \tag{76}$$

Comparing the obtained system of equations with Eq. (40), we conclude that

$$\beta_n^I = -\mathcal{V}_{n-1}^+, \quad \beta_n^{II} = \mathcal{V}_n^-. \tag{77}$$

This means that excess quantities following from non-equilibrium jump relations at the boundary between computational cells correspond directly to numerical fluxes in the conservative wave-propagation algorithm. Consequently, we can conclude that the wave-propagation algorithm is thermodynamically consistent.

The advantage of the wave-propagation algorithm is that every discontinuity in the parameters is taken into account by solving the Riemann problem at each interface between discrete elements. The algorithm in its thermodynamic representation was successfully applied to the solution of various problems (Berezovski and Maugin, 2001, 2002, 2003; Berezovski, Engelbrecht and Maugin, 2003; Berezovski, A., Berezovski, M., and Engelbrecht, 2006; Berezovski, Engelbrecht and Maugin, 2008; Berezovski, A., Berezovski, M., and Engelbrecht, 2009).

Heat conduction in one space dimension

As the next example, let us consider the construction of a numerical algorithm for heat conduction. In the simplest case with normalized heat capacity ($\rho C_p = 1$), the energy conservation can be represented as

$$\frac{\partial \theta}{\partial t} + \frac{\partial q}{\partial x} = 0, \tag{78}$$

where θ is temperature and q is the heat flux.

Following the approach described above, we introduce average (local equilibrium) and excess quantities both for temperature and heat flux

$$\theta = \bar{\theta} + \Theta, \quad q = \bar{q} + Q, \tag{79}$$

where, as previously, overbars denote averaged quantities and Θ and Q are the corresponding excess quantities.

Integration Eq. (78) over the computational cell gives

$$\frac{\partial}{\partial t}\int_{x_n}^{x_{n+1}} \theta dx = -q_n^+ + q_n^- = -\bar{q}_n - Q_n^+ + \bar{q}_n + Q_n^- = -Q_n^+ + Q_n^-. \tag{80}$$

Introducing the averaged temperature

$$\bar{\theta}_n = \frac{1}{\Delta x}\int_{x_n}^{x_{n+1}} \theta(x,t) dx, \tag{81}$$

and integrating over the time step, we arrive at

$$\bar{\theta}_n^{k+1} - \bar{\theta}_n^k = \frac{1}{\Delta x}\int_{t^k}^{t^{k+1}} -\left(Q_n^+ - Q_n^-\right) dt. \tag{82}$$

Calculating the integral in the right hand side of Eq. (82) by means of the trapezoidal rule, we arrive at the numerical scheme

$$\bar{\theta}_n^{k+1} - \bar{\theta}_n^k = -\frac{\Delta t}{2\Delta x}\left(\left(Q^+\right)_n^{k+1} + \left(Q^+\right)_n^k - \left(Q^-\right)_n^{k+1} - \left(Q^-\right)_n^k\right). \tag{83}$$

However, the values of the heat flux excess are not determined yet. To do this, let us consider jump relations at boundaries between computational cells. The first one follows from the continuity of temperature

$$[\![\bar{\theta} + \Theta]\!] = 0. \tag{84}$$

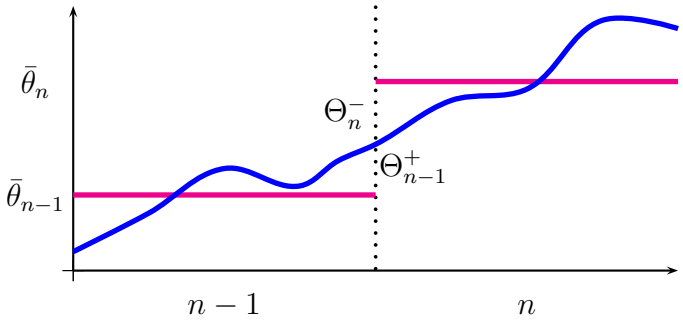

Figure 4. Temperatures at a boundary between cells.

The continuity of temperature should hold at any time step. It is instructive to represent the condition in the numerical form. At the left boundary we have

$$\bar{\theta}_{n-1}^k + \left(\Theta^+\right)_{n-1}^k = \bar{\theta}_n^k + \left(\Theta^-\right)_n^k, \quad \bar{\theta}_{n-1}^{k+1} + \left(\Theta^+\right)_{n-1}^{k+1} = \bar{\theta}_n^{k+1} + \left(\Theta^-\right)_n^{k+1}, \tag{85}$$

respectively. Similar relations hold at the right boundary

$$\bar{\theta}_n^k + \left(\Theta^+\right)_n^k = \bar{\theta}_{n+1}^k + \left(\Theta^-\right)_{n+1}^k, \quad \bar{\theta}_n^{k+1} + \left(\Theta^+\right)_n^{k+1} = \bar{\theta}_{n+1}^{k+1} + \left(\Theta^-\right)_{n+1}^{k+1}. \tag{86}$$

This is illustrated in Fig. 4.

Now we turn to heat flux. According to the Fourier's law, heat flux is proportional to the temperature gradient

$$q(x,t) = -k\frac{\partial\theta}{\partial x}. \tag{87}$$

Integration Eq. (87) over the computational cell leads to

$$\int_{x_n}^{x_{n+1}} q dx = -k\theta_n^+ + k\theta_n^- = -k(\bar{\theta}_n + \Theta_n^+ - \bar{\theta}_n - \Theta_n^-) = -k(\Theta_n^+ - \Theta_n^-). \tag{88}$$

The latter means that the average value of heat flux is determined by the difference of the temperature excess at the boundaries of the same computational cell

$$\bar{q}_n = \frac{1}{\Delta x}\int_{x_n}^{x_{n+1}} q dx = -\frac{k}{\Delta x}(\Theta_n^+ - \Theta_n^-). \tag{89}$$

The heat flux excess is assumed to be continuous

$$[\![Q]\!] = 0, \tag{90}$$

and determined by the difference of the temperature excess at the boundary of neighboring computational cells

$$Q_{n-1}^+ = Q_n^- = \frac{k}{\Delta x}(\Theta_n^- - \Theta_{n-1}^+). \tag{91}$$

The latter relation allows us to calculate the heat flux excess difference

$$Q_n^+ - Q_n^- = \frac{k}{\Delta x}(\Theta_{n+1}^- - \Theta_n^+ - \Theta_n^- + \Theta_{n-1}^+). \tag{92}$$

Due to the continuity of temperature we can represent the difference in terms of averaged temperatures

$$Q_n^+ - Q_n^- = \frac{k}{\Delta x}(\bar{\theta}_n - \bar{\theta}_{n+1} - \bar{\theta}_{n-1} + \bar{\theta}_n) = -\frac{k}{\Delta x}(\bar{\theta}_{n+1} + \bar{\theta}_{n-1} - 2\bar{\theta}_n). \tag{93}$$

The obtained relation between the heat flux excess difference and averaged temperatures holds true for each time step. Therefore, the numerical scheme (83) can be represented in terms of averaged temperatures as

$$\bar{\theta}_n^{k+1} - \bar{\theta}_n^k = \frac{k\Delta t}{2\Delta x \Delta x}(\bar{\theta}_{n+1}^{k+1} + \bar{\theta}_{n-1}^{k+1} - 2\bar{\theta}_n^{k+1} + \bar{\theta}_{n+1}^k + \bar{\theta}_{n-1}^k - 2\bar{\theta}_n^k). \tag{94}$$

The latter scheme is nothing else but the standard Crank-Nicolson method.

Conclusions

The main steps in the construction of a thermodynamically consistent numerical method are the following. Division of a body into a finite number of computational cells requires the description of all fields inside the cells as well as the interaction between neighboring cells. The state of each computational cell is associated with the corresponding local equilibrium state (and, therefore, temperature and entropy can be defined as usual). The local equilibrium approximation is achieved by averaging of all fields over the cell. The approximation of wanted fields inside the cells leads to discontinuities of the fields at boundaries between cells. This also leads to the appearance of excess quantities, which represent the difference between exact and approximate values of a field. Interaction between neighboring cells is described by means of fluxes at the boundaries of the cells. These fluxes are calculated by means of (non-equilibrium) jump relations at the boundaries between cells. Mathematically inspired well-established numerical methods are then recovered for wave propagation and heat conduction.

It should be noted that the thermodynamic representation of finite volume methods, which is formally identical to well-known numerical methods on smooth solutions, gives additional possibilities in the solution of problems with moving discontinuities (like cracks and phase-transition fronts) due to its ability to handle jump relations at discontinuities (Berezovski and Maugin, 2005, 2006; Berezovski et al., 2007; Berezovski, Engelbrecht and Maugin, 2008; Berezovski, 2008).

Acknowledgments

Support of the Estonian Science Foundation under grant No. 8702 is gratefully acknowledged.

References

Achenbach, J. D.: *Wave Propagation in Elastic Solids.* North-Holland, Amsterdam, 1973.

Bale, D. S., LeVeque, R. J., Mitran, S., Rossmanith, J. A.: A wave propagation method for conservation laws and balance laws with spatially varying flux functions. *SIAM J. Sci. Comp.* 24: 955–978, 2003.

Berezovski, A.: Influence of geometry and loading conditions on the martensitic front propagation. *Smart Struct. Syst.* 4: 123–135, 2008.

Berezovski, A., Berezovski, M., Engelbrecht, J.: Numerical simulation of nonlinear elastic wave propagation in piecewise homogeneous media. *Mater. Sci. Engng.* A 418: 364–369, 2006.

Berezovski, A., Berezovski, M., Engelbrecht, J.: Waves in Inhomogeneous Solids. In: *Applied Wave Mathematics - Selected Topics in Solids, Fluids and Mathematical Methods*, E. Quak, T. Soomere (Eds.), Springer, Berlin, pp. 55-81, 2009.

Berezovski, A., Berezovski, M., Engelbrecht, J., Maugin, G. A.: Numerical simulation of waves and fronts in inhomogeneous solids. In: *Multi-Phase and Multi-Component Materials under Dynamic Loading*, W.K.Nowacki and Han Zhao (Eds.), Inst. Fundam. Technol. Research, Warsaw, (EMMC-10 Conference), pp. 71-80, 2007.

Berezovski, A., Engelbrecht, J., Maugin, G. A.: Numerical simulation of two-dimensional wave propagation in functionally graded materials. *Eur. J. Mech. - A/Solids* 22: 257–265, 2003.

Berezovski, A., Engelbrecht, J., Maugin, G. A.: *Numerical simulation of waves and fronts in inhomogeneous solids.* World Scientific, Singapore, 2008.

Berezovski, A., Maugin, G. A.: Simulation of thermoelastic wave propagation by means of a composite wave-propagation algorithm. *J. Comp. Physics* 168: 249–264, 2001.

Berezovski, A., Maugin, G. A.: Thermoelastic wave and front propagation. *J. Thermal Stresses* 25: 719–743, 2002.

Berezovski, A., Maugin, G. A.: Simulation of wave and front propagation in elastic and thermoelastic heterogeneous materials. *Comput. Mater. Sci.* 28: 478–485, 2003.

Berezovski, A., Maugin, G. A.: Stress-induced phase transition front propagation in thermoelastic solids *Eur. J. Mech.- A/Solids* 24: 1–21, 2005.

Berezovski, A., Maugin, G. A.: Numerical simulation of phase-transition front propagation in thermoelastic solids. In: *Numerical Mathematics and Advanced Applications* (Proceedings of ENUMATH 2005), A. Bermudez de Castro, D. Gomez, P. Quintela, P. Salgado (Eds.), Springer, Berlin, pp. 703-711, 2006.

Fogarthy, T., LeVeque, R. J.: High-resolution finite-volume methods for acoustics in periodic and random media. *J. Acoust. Soc. Am.* 106: 261–297, 1999.

Godlewski, E., Raviart, P.-A.: *Numerical Approximation of Hyperbolic Systems of Conservation Laws*. New York, Springer, 1996.

Guinot, V.: *Godunov-type Schemes: An Introduction for Engineers*. Elsevier, Amsterdam, 2003.

Hoffmann, K. H., Burzler, J. M., Schubert, S.: Endoreversible thermodynamics. *J. Non-Equil. Thermodyn.* 22: 311–355, 1997.

Langseth, J. O., LeVeque, R. J.: A wave propagation method for three-dimensional hyperbolic conservation laws. *J. Comp. Physics* 165: 126–166, 2000.

LeVeque, R. J.: Wave propagation algorithms for multidimensional hyperbolic systems. *J. Comp. Physics* 131: 327–353, 1997.

LeVeque, R. J.: Balancing source terms and flux gradients in high-resolution Godunov methods: the quasi-steady wave-propagation algorithm. *J. Comp. Physics* 148: 346–365, 1998.

LeVeque, R. J.: *Finite Volume Methods for Hyperbolic Problems*. Cambridge University Press, 2002.

Lienhard, John H. IV, Lienhard, John H. V: *A Heat Transfer Textbook*. Third Edition, Phlogyston Press, Cambridge MA, 2004.

Muschik, W., Berezovski, A.: Thermodynamic interaction between two discrete systems in non-equilibrium. *J. Non-Equilib. Thermodyn.* 29: 237–255, 2004.

Stoker, J. J.: *Water Waves: The Mathematical Theory With Applications*. Interscience, New York, 1957.

Thompson, P. A.: *Compressible Fluid Flow*. McGraw-Hill, New York, 1972.

Toro, E. F.: *Riemann Solvers and Numerical Methods for Fluid Dynamics*. Springer, Berlin, 1997.

Toro, E. F. (ed.): *Godunov Methods: Theory and Applications*. Kluwer, New York, 2001.

Arkadi Berezovski
Centre for Nonlinear Studies
Institute of Cybernetics at Tallinn University of Technology
Akadeemia tee 21
Tallinn, 12618, Estonia
Arkadi.Berezovski@cs.ioc.ee